AIAA JOURNAL
Vol. 44, No. 11, November 2006

Active Trailing-Edge Flap Control of Oscillating-Wing Tip Vortex

P. Gerontakos* and T. Lee†
McGill University, Montreal, Quebec H3A 2K6, Canada

DOI: 10.2514/1.19776

The tip vortex generated by an oscillating NACA 0015 wing with a moveable trailing-edge flap was investigated at $Re = 1.65 \times 10^5$ by using a miniature triple hot-wire probe. Both positive and negative flap deflections, actuated at different start times, were tested. The negative flap motion was found to be most effective in displacing the vortex position with earlier actuations leading to larger vertical vortex displacements. Negative flap deflections strengthened the vortex, moved the centroid further outboard, decreased the peak vorticity ζ_{peak}, and increased the vortex size. The positive trailing-edge flap motion, however, resulted in a more concentrated tip vortex of reduced vortex strength Γ_o located further inboard. The lift-induced drag was decreased (increased) for positive (negative) trailing-edge flap, compared to a baseline wing.

Nomenclature

b	=	(semi-)wing span
C_{Di}	=	lift-induced drag coefficient, $=D_i/\frac{1}{2}\rho u_\infty^2 S$
C_l	=	section lift coefficient
C_m	=	section pitching-moment coefficient
C_p	=	surface pressure coefficient
C_w	=	torsional damping factor
c	=	airfoil chord
f_o	=	oscillation frequency
Re	=	Reynolds number, $=u_\infty c/\nu$
S	=	wing area
t	=	time
t_d	=	flap actuation duration
t_e	=	flap actuation end time
t_s	=	flap actuation start time
t_{ss}	=	steady-state time period
u	=	mean wake velocity
u_c	=	axial core velocity
u_∞	=	freestream velocity
x, y, z	=	streamwise, normal, and spanwise distances
α	=	angle of attack
α_{ds}	=	dynamic-stall angle
α_{ms}	=	dynamic moment-stall angle
α_{ss}	=	static-stall angle
Γ	=	vortex strength or circulation
Γ_o	=	total circulation
$\delta_{\max}$	=	maximum flap deflection
ζ	=	streamwise vorticity
κ	=	reduced frequency, $=\pi f_o c/u_\infty$
ν	=	kinematic viscosity
v_θ	=	tangential velocity
ρ	=	fluid density

Subscripts

d	=	pitch-down
u	=	pitch-up

Received 1 September 2005; revision received 12 June 2006; accepted for publication 14 June 2006.

*Graduate Research Assistant, Department of Mechanical Engineering.
†Associate Professor, Department of Mechanical Engineering, Member AIAA.

Introduction

WING tip vortices, because of their hazardous effects on flight safety and airport capacity, continue to be of concern to the aviation industry and aircraft manufacturers. For rotorcraft, when these shed concentrated vortices interact with the trailing rotor blades, the unsteady pressure fluctuations induced on the blade surfaces generally lead to severe dynamic structural loading and impulsive blade-vortex-interaction (BVI) noise generation. The rotorcraft BVI noise is highly complex, 3-D, and time dependent, and is particularly evident and generally dominant during a low-speed descent flight, as in landing approach and during maneuvers, where the rotor disk travels through its own wake.

Two important blade-vortex interaction extremes occur when the vortex is either normal, which affects a small spanwise portion of the airfoil, or parallel, which affects most of the airfoil and generates the greatest effect on BVI noise, to the airfoil. Past experimental and computational results [1–5] indicated that the more nearly parallel the tip vortex is to the blade at the time of interaction, the more intense the noise, and that the blade-vortex interactions are highly dependent on the rotor's wake structure and trajectory. Hardin and Lamkin [1] showed theoretically that the severity of the acoustic pressure time history $p(x, t)$ produced by the BVI phenomenon can be expressed as

$$p(x, t) \approx \Gamma L l/\rho_\infty d_{\text{miss}}^2 \tag{1}$$

where x is the observer position in the airfoil fixed coordinate system, Γ is the intensity of the incoming vortex, L is the lift of the blade (per unit length) at the time of interaction, l is the span over which essentially the 2-D interaction occurs, d_{miss} is the miss distance of the vortex (which is controlled by the vortex trajectory), and ρ_∞ is the freestream density. Various passive and active control devices [6–13] have been attempted to modify the shed vortex structure (i.e., Γ, l, and d_{miss}) at the time of the vortex generation and/or at the time of vortex interaction by changing the blade tip shape, adding other aerodynamic surfaces mounted at the rotor tip (such as winglets, spoiler, and stub/subwing), or by the use of active higher harmonic control, individual blade control, and trailing-edge flaps/tabs. Among them, the active plain trailing-edge flap, integrated with the main lifting section of the blade and deflected cyclically so as to change the lift and/or moment characteristics of the blade section, has been proposed by researchers elsewhere for both primary control (i.e., swashplateless pitch control [12]) and active vibration and noise control [13]. Enenkl et al. [13] suggested that the way an active trailing-edge flap reduces noise and vibration may vary, depending mainly on the flap chord, control frequency, and the blade's torsional stiffness. The details of the vortex flow characteristics, however, were not reported.

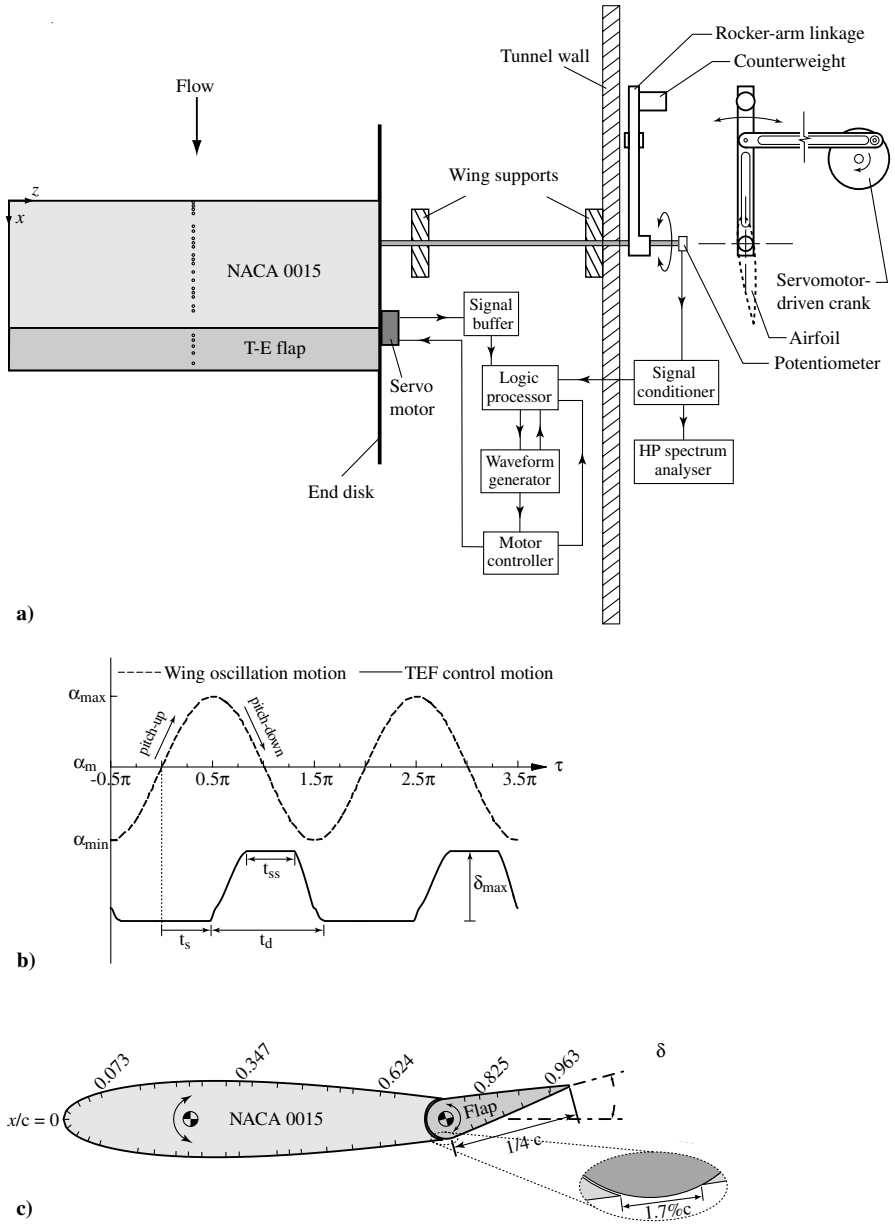

Fig. 1 a) Schematics of wing model and experimental setup; b) definition of flap actuation start time t_s, duration t_d, and amplitude $\delta_{\max}$; and c) surface pressure orifice locations.

In addition, it is also of importance to note that active trailing-edge flaps have also been proposed to alleviate the undesirable nose-down pitching moment observed on dynamically stalled helicopter rotor blades [14,15], as well as to enhance the leading-edge vortex (LEV)-induced lift overshoot of a rapidly pitching wing [16]. The occurrence of dynamic-stall induced overshoots in lift and drag forces and the accompanied high torsional and pitch control loads on helicopter rotor blades continues to make dynamic stall and its control an important topic in rotorcraft engineering. It is now known that the predominant features of dynamic stall are the formation, convection, and shedding over the upper surface of the airfoil of an energetic LEV, which induces a nonlinearly fluctuating pressure field and produces large transient variations in forces and moments that may be many times larger than their static counterparts. An excellent review is given by McCroskey [17]. It is therefore believed that the transient LEV phenomenon will greatly influence the

Table 1 TEF motion profile parameters and critical aerodynamic values. 14°_u denotes $\alpha_u = 14°$; 14°_d denotes $\alpha_d = 14°$; $t_d = 50\% f_o^{-1}$; $t_{ss}/t_d = 0.36$

$\delta_{\max}$	t_s	t_s	t_e	t_e	$C_{l,\max}$	α_{ds}	$C_{d,\max}$	α_{ms}	$C_{m,\text{peak}}$	$C_{w,\text{ccw}}$	$C_{w,\text{cw}}$	$C_{w,\text{net}}$
TEF control:												
+7.5°	-0.5π	8°	0.5π	20°	1.18	20.0°	0.40	19.7°	−0.117	0.04	−1.07	−1.04
+7.5°	0.0π	14_u°	1.0π	14_d°	1.07	19.9°	0.33	19.2°	−0.057	0.10	−0.48	−0.38
+7.5°	0.5π	20°	-0.5π	8°	1.22	19.8°	0.41	19.1°	−0.123	0.35	−0.14	0.21
−7.5°	-0.5π	8°	0.5π	20°	1.35	19.7°	0.42	19.1°	−0.130	0.35	−0.09	0.26
−7.5°	0.0π	14_u°	1.0π	14_d°	1.44	19.8°	0.52	19.1°	−0.213	0.12	−0.19	−0.07
−7.5°	0.5π	20°	-0.5π	8°	1.25	20.0°	0.45	19.5°	−0.181	0.04	−0.89	−0.85
Baseline wing:					1.23	19.9°	0.40	19.2°	−0.119	0.11	−0.42	−0.31
Static wing:					0.95	16.5°	0.12	16.5°	−0.023	——	——	——

behavior of the tip vortex. However, unlike the considerable experimental and numerical efforts made toward the understanding and control of the tip vortex generated by a fixed-wing tip, only limited results have been reported, to the authors' knowledge, on the tip vortex generated behind an oscillating wing with no control [18,19].

The objective of this study was to use a full-span trailing-edge flap (TEF) flow-control actuator to control the tip vortex flow characteristics in the near field behind an oscillating NACA 0015 airfoil at $Re = 1.65 \times 10^5$ by using a miniature triple hot-wire probe. Three prescheduled TEF motions, superimposed on the sinusoidally oscillated wing, were tested. Both positive and negative flap deflections were tested. Special emphasis was placed on the characterization of the effects of the TEF actuation start time and deflection direction on the strength, size, shape, and trajectory of the shed tip vortex. Phase-locked ensemble-averaged crossflow and axial velocity fields and the vorticity distribution of the vortex over one cycle of oscillation were also investigated. Dynamic-load loops, obtained by integrating the unsteady surface pressure measurements were also obtained to supplement the tip vortex data. The effect of the TEF control scheme on the potential mitigation of the severity of the blade-vortex interaction was also discussed.

Experimental Methods

The experiment was conducted in the 0.9 m × 1.2 m × 2.7 m low-speed, suction-type wind tunnel at McGill University with a freestream turbulence intensity of 0.03% at $u_\infty = 35$ m/s. A square-tipped, rectangular, untwisted NACA 0015 airfoil, fabricated from solid aluminum, with a chord length c of 25.4 cm and a semispan b of 38 cm, was used as the test model. The wing model was mounted horizontally at the center of the wind tunnel test section. A 40-cm diameter aluminum endplate with a sharp leading edge was fixed to an end support located 22 cm from the sidewall of the test section. The gap between the wing and the endplate was kept at less than 1 mm to minimize the leakage flow through the gap. The origin of the

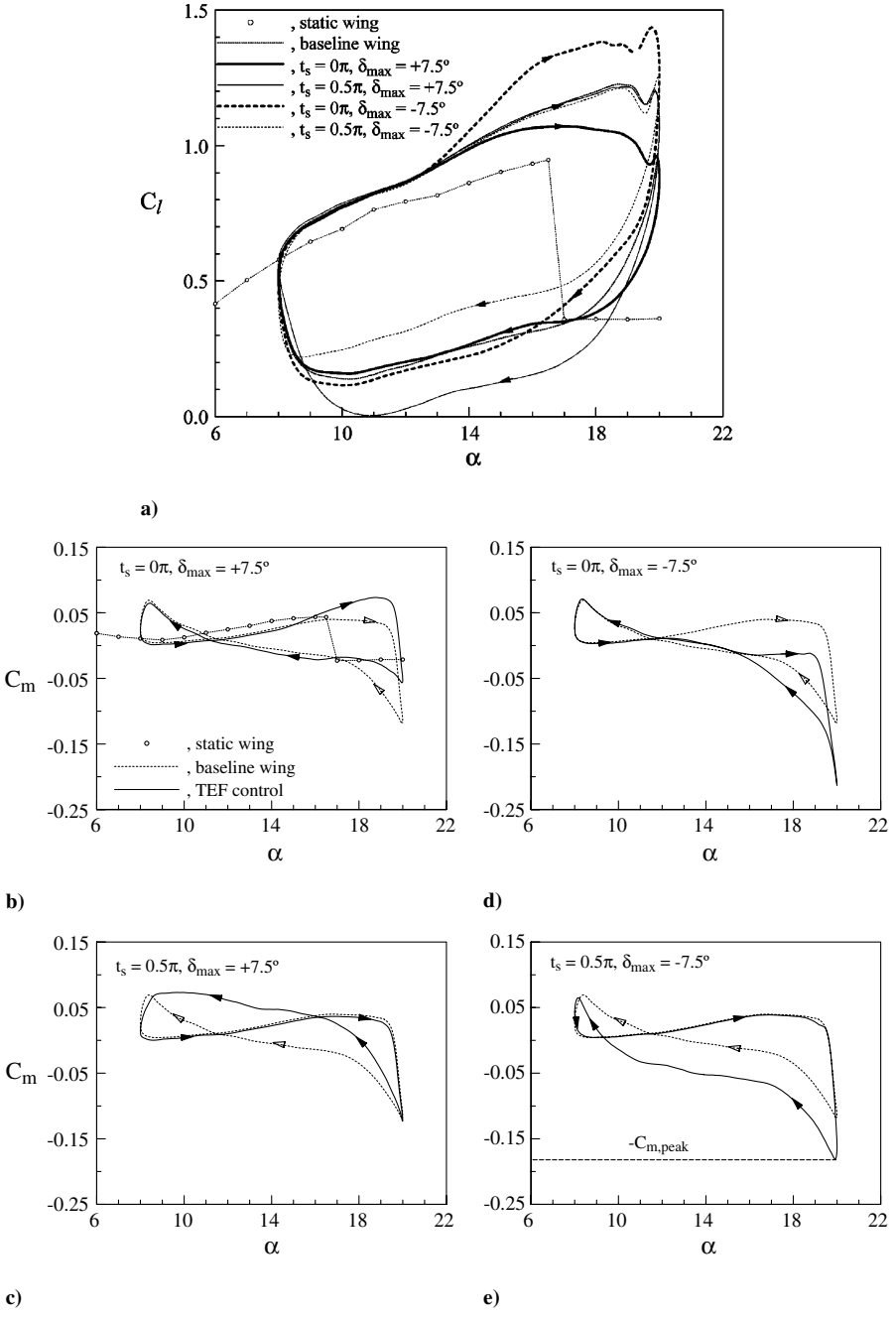

Fig. 2 Effect of TEF control on dynamic C_l and C_m loops.

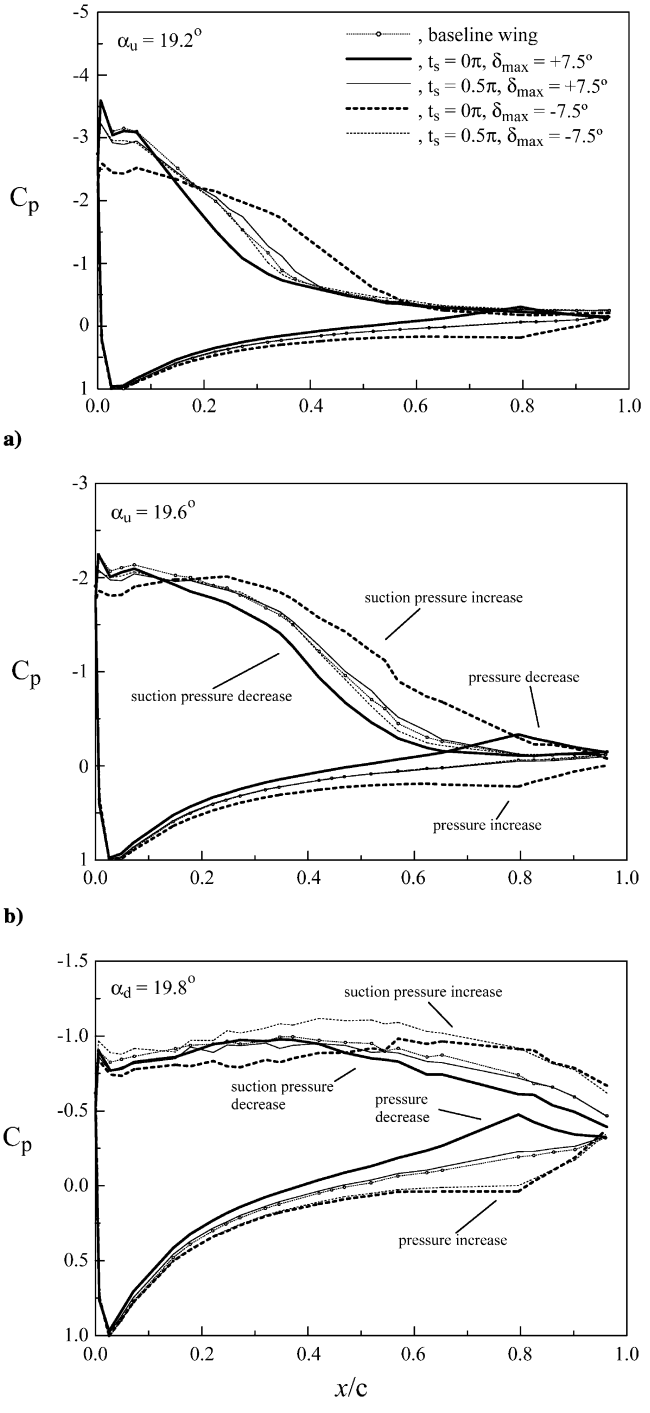

Fig. 3 Typical C_p distributions with and without TEF control.

coordinates was located at the wing-tip leading edge with x, y, and z in the streamwise, normal, and spanwise directions, respectively. The freestream velocity u_∞ was fixed at 10.1 m/s, which rendered a chord Reynolds number of 1.65×10^5.

A specially designed four-bar linkage and flywheel oscillation mechanism, capable of oscillating the airfoil sinusoidally at various amplitudes and frequencies, mounted on the external of the wind tunnel was used in the present experiment (Fig. 1a). The oscillating wing was chosen to simulate the quasiperiodic first harmonic angle of attack variations that are found on helicopter rotors during low-speed forward flight. The mean angle of attack α_m was varied by changing the relative angle between the rotating shaft and the rocker-shaft connector. The oscillation amplitude $\Delta\alpha$ was varied by attaching the coupler at specific radial locations on the flywheel. The flywheel was attached directly to an Exlar model DXM340C servomotor driven by an Emerson model FX3161 PCM1 programmable motion controller. The oscillation frequency f_o was monitored in real time using a HP model 3581A spectral analyzer and was measured to an accuracy of ± 0.02 Hz. The four-bar mechanism provided an output which was sinusoidal to within 2%. The airfoil pitch axis was located at the 1/4-chord location. The instantaneous airfoil incidence and the phase reference signal $\tau = \omega t$ were recorded from both the servomotor feedback resolver and a potentiometer mounted on the servomotor shaft. In the present experiment, the wing was oscillated through the 2-D static-stall angle $\alpha_{ss} = 16.5^\circ$ with $\alpha(t) = 14^\circ + 6^\circ \sin \omega t$ and a reduced frequency κ of 0.1. Note that when the phase angle was within the range $-0.5\pi \le \tau \le 0.5\pi$, the wing was described to be in pitch-up; when $0.5\pi \le \tau \le 1.5\pi$, the wing was said to be in pitch-down. Also, in the following discussion, the suffix u is used to indicate pitch-up when α is increasing and d is used to indicate pitch-down when α is decreasing.

The wing was equipped with a 25%c full-span TEF of a simple-hinged type. The TEF was activated and deactivated independently by a Futaba model S-3003 servomotor located at the wing root and driven by a custom-built controller (Fig. 1a), which actuated the flap in response to the wing phase signal. The TEF actuation employed a brief pulse and was actuated at any desired time and instantaneous angle of attack. The servomotor motion was represented by a constant ramp-up motion, remained steady briefly, and was followed by a constant ramp-down motion (Fig. 1b). The ramp-up and ramp-down times were each approximately 7% of the time required for the wing to undergo one full cycle of oscillation. The TEF actuation start time t_s and deflection direction were tested independently to quantify their effects on the dynamic-stall lift coefficients and the tip vortex flow structure. Both positive (or upward) and negative (or downward) flap deflections with $\delta_{max} = \pm 7.5^\circ$ were tested. The magnitude of δ_{max} was limited by the required oscillation frequency of the main wing, as well as by the present TEF actuation mechanism. Three different $t_s = -0.5\pi$, 0π, and 0.5π radians, corresponding to the flap actuation initiated at α_{min}, α_m, and α_{max}, respectively, with $t_d = 50\% f_o^{-1}$ (i.e., the flap actuation duration accounted for 50% of the oscillation cycle) were considered. Note that for the start time $t_s = 0\pi$ control case, the flap was actuated at around the onset of flow reversal [20]. Details of the parameters describing the flap actuation profile in various units are given in Table 1.

The NACA 0015 wing model was also equipped with 48 0.35-mm-diameter pressure taps, covering $x/c = 0$ to 96.3%, distributed evenly over the upper and lower surfaces of the wing model (Fig. 1c). The orifices, located along the midspan of the airfoil, were staggered 1.5 mm apart in the spanwise direction to avoid the wake effect from an upstream orifice on orifices further downstream. The pressure signals, recorded using a fast-response Honeywell DRAL501 differential pressure transducer (with a range of 50 mm of water head) connected via a 48-port scanivalve system, were phase locked ensemble averaged over 75 cycles of oscillation and were integrated numerically to compute the unsteady aerodynamic loads and pitching moments. The dynamic range of the pressure transducer was on the order of 10 kHz. The transducer signals were low pass filtered (250 Hz) and amplified with a multichannel AA Lab model G3006 pressure measurement system. The effects of the 35-cm long and 0.75-mm i.d. plastic tubing, separating the surface tap and the pressure transducer, on the unsteady pressure signals were examined by comparing the transducer output level and the phase with a controlled acoustic sound source. The effect of the length of the plastic tubing was found to be a simple time constant delay on all pressure signals with frequency above 2.95 Hz, which rendered a limited reduced frequency κ of 0.233 at $u_\infty = 10.1$ m/s or $Re = 1.65 \times 10^5$ in the present experiment. Details of this method can be found in the work of Rennie and Jumper [16] and Lee and Gerontakos [20]. An uncertainty analysis gives a typical total uncertainty ± 0.013 in C_p. Note that for the surface pressure measurements, two end plates were used to ensure a 2-D flow over the wing model. The two-dimensional uniformity of the flow distribution over the wing model was checked by traversing a 5-μm normal hot-wire probe, located at 30%c downstream from the

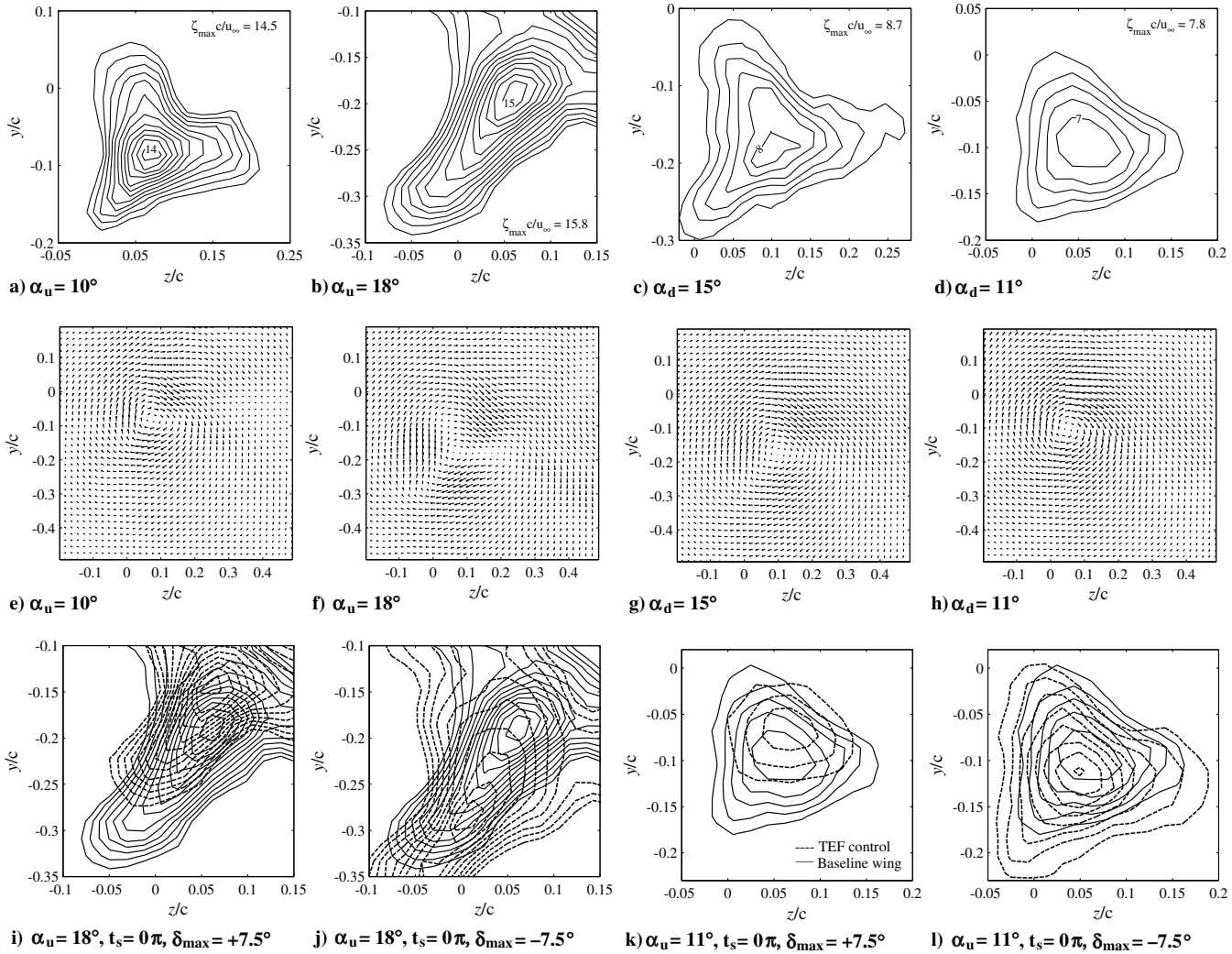

Fig. 4 Representative normalized isovorticity contours and velocity vector plots. a)–h): baseline wing; i)–l): comparison of wing with and without TEF control. $\Delta\zeta c/u_\infty = 1$.

leading edge of the wing and $y = 5$ mm above the airfoil, along the span. The nonuniformity was found to be $\pm 3\%$ of the freestream value.

The instantaneous velocities of the tip vortex were measured by a miniature triple hot-wire probe (Auspex Model AVEP-3-102 with a measurement volume of 0.5 mm^3), and were subsequently ensemble averaged over 40–80 oscillating cycles to obtain phased-locked averages of the flow properties at various phase positions during the cycle. The triple hot-wire probe was calibrated in situ, following the calibration procedures described by Chow et al. [21], before the installation of the model. The hot-wire signals were sampled at 500 Hz and were recorded on a PC through a 16-bit A/D converter board. Probe traversing was achieved through a custom-built computer-controlled traversing system. The three-dimensional velocities downstream of the trailing edge of the wing were measured in planes perpendicular to the freestream velocity at $x/c = 2.5$ (relative to the leading edge). Data planes taken in the near field of the wing models had 33×34 measuring grid points with an increment of $\Delta y = \Delta z = 3.2$ mm. The maximum experimental uncertainties in the results reported have been estimated as follows: mean velocity 3.5%, vorticity component 8%, vortex radius 4%, and velocity fluctuation 3%.

Results and Discussion

Dynamic C_l and C_m Loops

To facilitate the investigation of the effects of TEF motion on the tip vortex flow structure, the phase-locked ensemble-averaged dynamic-C_l and -C_m loops of the 2-D NACA 0015 airfoil oscillated with $\alpha(t) = 14^\circ + 6^\circ \sin \omega t$ and $\kappa = 0.1$ (for $t_s = -0.5\pi$, 0π, and 0.5π radians, $\delta_{\max} = \pm 7.5^\circ$ and $t_d = 0.5 f_o^{-1}$) were investigated first and served as an experimental guideline. Figure 2 shows clearly that for an uncontrolled or baseline wing, the dynamic maximum lift coefficient $C_{l,\max}$ (at $\alpha_{ds} = 19.9^\circ$) was about 0.28 higher than the static-stall value (at $\alpha_{ss} = 16.5^\circ$), but the large nose-down pitching moment was of more significance; a 5.2 times increase in $|-C_{m,\text{peak}}|$ was observed. With TEF control, a pronounced variation in the C_l and C_m curves, compared to a baseline wing, can be clearly seen. For a positive flap deflection, there was a reduction in C_l (Fig. 2a) and $|-C_m|$ (Figs. 2b and 2c), as a result of the TEF-induced negative camber in the trailing-edge region. Furthermore, provided the flap remains deflected throughout the stalling process, the magnitudes of $C_{l,\max}$ and $|-C_{m,\text{peak}}|$ are considerably diminished. A 13% and 52% reduction in $C_{l,\max}$ and $|-C_{m,\text{peak}}|$, respectively, was observed for the $t_s = 0\pi$ (i.e., flap actuation at around the onset of flow reversal) and $\delta_{\max} = +7.5^\circ$ TEF control case, compared to a baseline wing, showing that the upward TEF deflection primarily provided a mitigation of the excessive nose-down C_m produced by the transient LEV effects. For $t_s = 0.5\pi$ (i.e., flap deflection actuated at $\alpha_{\max}$), the C_l and C_m curve, including the magnitude of the peak negative pitching-moment coefficient, remained unchanged during pitch-up, as expected, while the post-stall lift loss was increased, compared to a baseline wing. The value of the net torsional damping factor $C_{w,\text{net}}$ could, however, be increased considerably, as a result of the presence of the large C_w loop in the C_m-α curve. That is, the magnitude of $-C_{m,\text{peak}}$ may remain unchanged, while the $C_{w,\text{net}}$ might become

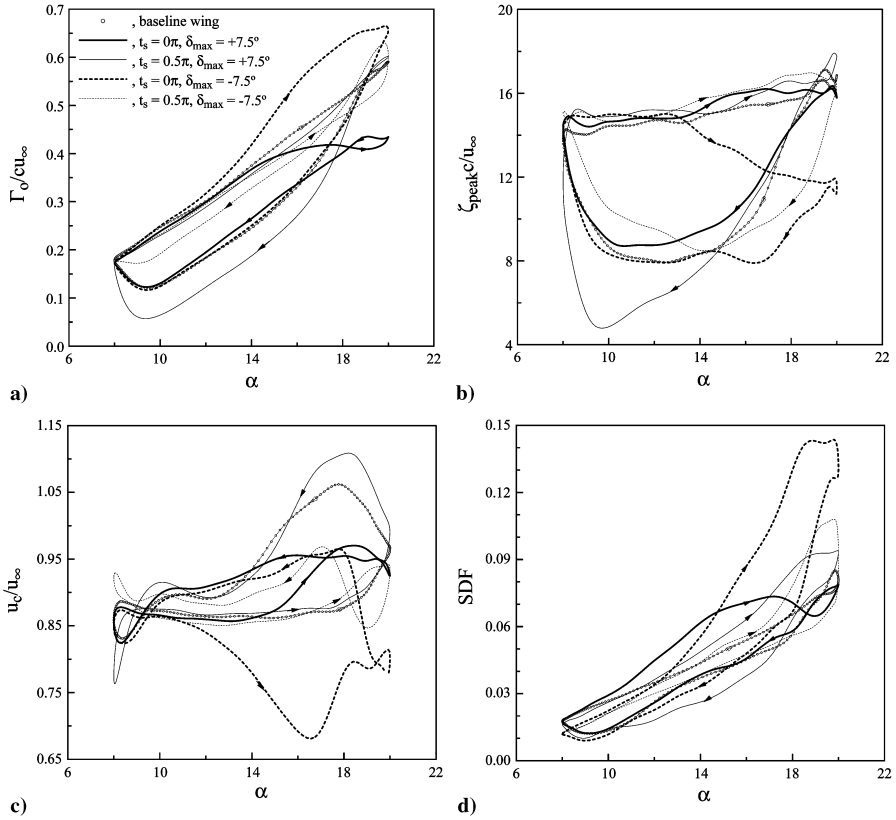

Fig. 5 Dynamic loops of normalized total circulation, peak vorticity, axial core velocity, and vortex shape distortion factor (SDF).

positive. The torsional damping factor was defined by the line integral [22]

$$C_w = \int C_m(\alpha)\,\mathrm{d}\alpha = \int_{\mathrm{ccw}} C_m(\alpha)\,\mathrm{d}\alpha + \int_{\mathrm{cw}} C_m(\alpha)\,\mathrm{d}\alpha \qquad (2)$$

C_w is positive when it corresponds to a ccw (counterclockwise) loop while negative for a cw (clockwise) loop in the C_m versus α curve. The values of the critical aerodynamic flow features, including the C_w values, for both controlled and uncontrolled TEF conditions are listed in Table 1. The results indicate that the later the actuation the net torsional damping was improved and passed from negative to positive for the latest actuation time. The post-stall lift loss and the degree of hysteresis were also found to increase with increasing t_s.

It is also interesting to note that the underlying physics responsible for the observed decrease in $C_{l,\max}$ and $|-C_{m,\mathrm{peak}}|$ for positive flap deflection was found to be mainly attributed to the unexpected presence of suction pressure on the "lower" surface of the flap (Fig. 3), and, to a lesser extent, to the reduction in the suction pressure on the upper surface of the wing, compared to a baseline wing. This pressure difference or imbalance contributed to the increment of the nose-up pitching moment. The surface pressure distributions also show that for a flap actuated during pitch-up (i.e., $t_s = -0.5\pi$ and 0π), the angles of attack at which the formation, convection, and detachment of the LEV was found to be virtually unaffected by the upward TEF motion. The low pressure signature or footprint of the LEV was, however, reduced by the positive flap deflection (Figs. 3a–3c), compared to a baseline wing, especially in the trailing-edge region.

For negative (or downward) TEF motions ($\delta_{\max} = -7.5^\circ$), the boundary-layer thickness was suppressed, especially in the vicinity of the trailing-edge region, and the flow remained attached to the upper surface of the airfoil to the highest possible α, compared to a baseline wing. The negative flap deflection-induced positive camber also shifted the lift-curve upward and caused a considerable increase in $C_{l,\max}$, although the α at which the $C_{l,\max}$ occurred was slightly decreased (Fig. 2a). In contrast to a positive TEF, the negative flap deflection also translated into an increase in suction pressure on the upper wing surface, as well as a substantial increase in the pressure on the pressure surface (Fig. 3) as compared to a baseline wing. As expected, the observed increase in pressure differential, which rendered the increase in C_l and $C_{l,\max}$, was also accompanied by a substantially intensified peak nose-down pitch moment, compared to a baseline wing as well. Considerable decrease in the hysteresis in the lift curve was observed for the $t_s = 0.5\pi$ case. For negative TEF motion, the earlier the flap actuation the more positive the net torsional damping and the larger the $C_{l,\max}$ and the $|-C_{m,\mathrm{peak}}|$, provided the occurrence of dynamic stall and flap deflection overlap.

In summary, depending on the values of t_s and $\delta_{\max}$, trailing-edge flaps could produce significant pitching-moment and lift changes. Negative TEF motions generated favorably additional lift, which in turn reduces the required rotor blade pitch angles, but at the price of an increased nose-down pitching moment. Deflection upward, or positively, generated adverse negative lift but provided favorable reduction in nose-down C_m control. For a flap actuated during pitch-up, the LEV formation and detachment were not affected, whereas the low pressure signature or footprint of the LEV was, however, reduced or increased, depending on the sign of $\delta_{\max}$. It is obvious that the observed TEF modification of the blade lift and pitching moment and, subsequently, the blade pitch, should also have a marked influence on the structure, strength, and trajectory (i.e., the equivalent of miss distance during BVI) of the tip vortex thus generated.

Effects of TEF on the Tip Vortex

The influence of the TEF motion on the tip vortex structure can be best manifested by the obvious changes in the shape and distribution of the nondimensional isovorticity contours $\zeta c/u_\infty$ (Fig. 4) and, consequently, the strength of the vortex (Fig. 5a). Figures 4a–4d present the typical reduction in the ζ-contour levels and the increase in the diffusion and size of the vortex at selected $\alpha_u = 10^\circ$ and 18° and $\alpha_d = 15^\circ$ and 11°, corresponding to the attached flow, during stall, post-stall, and flow reattachment flow regimes over an oscillation cycle of a baseline wing. The hysteretic property and increase–decrease trend present in the total circulation Γ_o loops between pitch-up and pitch-down, similar to the behavior of the

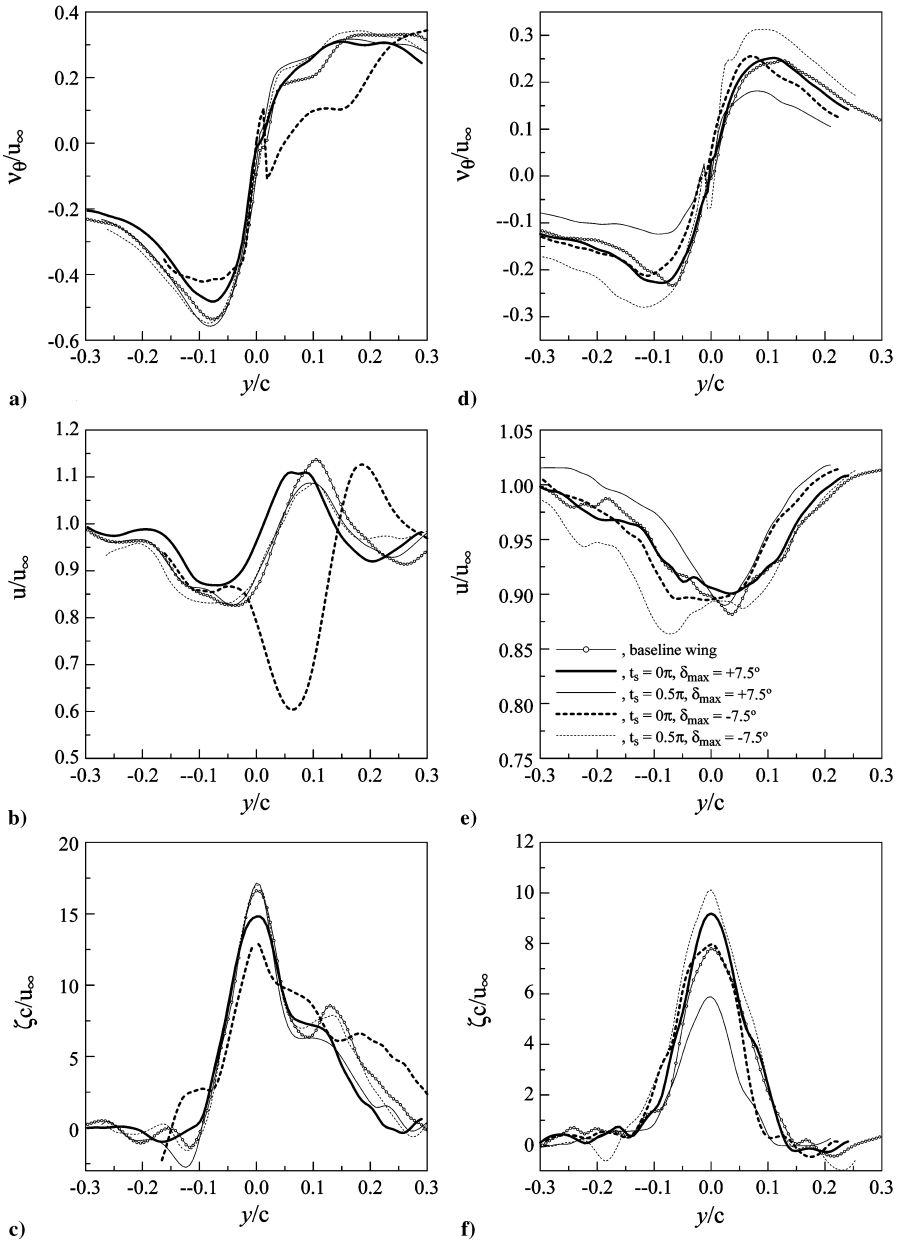

Fig. 6 Typical vortex flow quantities across the vortex center along the *y* axis. a)–c): $\alpha_u = 18°$; d)–f): $\alpha_d = 11^\circ$.

dynamic-C_l loop shown in Fig. 2, can be clearly seen (Fig. 5a). The corresponding normalized velocity vector plots are also presented in Figs. 4e–4h. The values of Γ_o were higher during pitch-up than during pitch-down, as a result of the LEV-induced separation and the asymmetry between the occurrence of the flow separation and reattachment. The circulation, or vortex strength, was calculated by the area integral over vorticity. The area integral was evaluated by summing the vorticity multiplied with the incremental area of the measuring grid. Figure 5b shows that the unsteady wing motion and the LEV transient effects also led to a minor increase in the core or peak vorticity ζ_{peak} during pitch-up. ζ_{peak}, however, started to decrease drastically during the first stage of pitch-down (i.e., during LEV detachment and the during-stall flow processes), reaching a local minimum, and began to rise (in the vicinity of $\alpha_d \approx 10^\circ$ which corresponded to the onset of flow reattachment) to the value of $\alpha_{\min}$ (Fig. 5b). Note also that because of the convection time required for a tip vortex to propagate from the wing to the downstream location of the measuring probe, there is a phase lag between any instantaneous probe reading and the position of the wing at that instant. In the present experiment, the convection speed of the vortex u_{conv} was approximated as the upper-bound freestream speed, because it resulted in the smallest phase-lag correction; a phase-lag compensation scheme suggested by Chang and Park [19]. The measurements reported in this study were phase lag compensated by letting $u_{\text{conv}} = u_\infty$.

With TEF control, large variations in ζ distribution and in the values of ζ_{peak} and Γ_o were observed. For a flap deflected upward during pitch-up, a considerable decrease in Γ_o (Fig. 5a), accompanied by a more tightly wound vorticity distribution (Figs. 4i–4k) and a minor increase in ζ_{peak} (Fig. 5b), compared to a baseline wing, was observed. Significant reduction in Γ_o and ζ_{peak} also exhibited for a flap deflected upward during the pitch-down motion of the wing (i.e., $t_s = 0.5\pi$); the unexpected large reduction in Γ_o during the during-stall flow process could be attributed to the fact that for the present light-stall wing oscillation, the extent of LEV-induced flow separation was rather limited, as a result of premature LEV growth and detachment, in contrast to the massive flow separation of a deep-stall wing oscillation, thus allowing the positive camber effects and the unloading of the tip vortex region, induced by the upward TEF motion, to remain effective. The substantial reduction in Γ_o also suggests that the positive TEF deflection was very effective in the alleviation of the strength of a tip vortex (or equivalently the severity of blade-vortex interactions), in addition to the improvement in the undesirable nose-down pitching moment, as

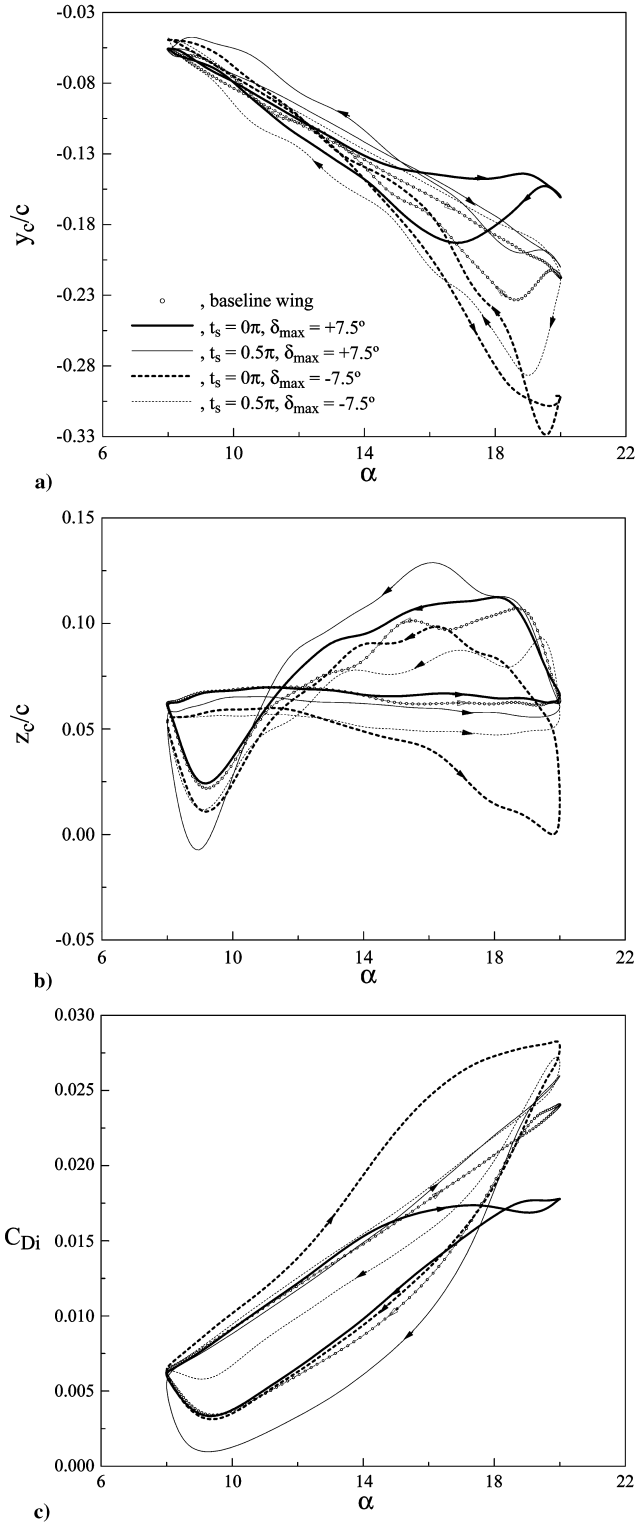

Fig. 7 a), b): vortex position and c) lift-induced drag coefficient.

shown in Figs. 2b and 2c, by virtue of the increased degree of spread of the vorticity (i.e., a less tightly wound or a more diffused tip vortex), compared to a baseline wing. The later the flap actuation the lower the vortex strength and the larger the hysteresis.

Figure 5a also shows that, as expected, negative TEF deflections always rendered a dramatic increase in Γ_o, regardless of the magnitude of t_s. The increase in Γ_o was, however, found to be accompanied by a reduction in ζ_{peak} as well as a more diffuse vortex, compared to a baseline wing (Figs. 4j–4l). The extent to which vortex strength, peak vorticity, and the hysteretic property were controlled depends on the flap actuation start time. Particular attention should also be given to the drastic reduction in the hysteresis in the Γ_o-α loop for a TEF actuated at $t_s = 0.5\pi$ with $\delta_{max} = -7.5^\circ$. Also, note that similar to a baseline wing, the total circulation and core vorticity had larger values during pitch-up than during pitch-down, and that the axial core velocity was higher during pitch-down than during pitch-up.

Figure 5c shows that for positively deflected TEF actuated at $t_s = 0\pi$ (i.e., at $\alpha_u = \alpha_m = 14^\circ$), the axial flow was always wakelike, while exhibiting a jetlike flow, similar to that of a baseline wing, for a flap actuated at $t_s = 0.5\pi$. On the other hand, u_c was consistently wakelike (of value significantly below that of a baseline wing) for downward TEF, regardless of the magnitude of t_s; a local minimum of $u_c = 0.68u_\infty$ at $\alpha_d \approx 16.5^\circ$, compared to $u_c = 0.87u_\infty$, was observed. The decrease of the vortex centerline velocity, to below the freestream value, with TEF control can be explained qualitatively using Batchelor's analysis [23]. The axial velocity on the centerline can be written as

$$u/u_\infty = \{1 + [(p_\infty - p) - \rho g \Delta H]/\tfrac{1}{2}\rho u_\infty^2\}^{1/2} \tag{3}$$

where $p_\infty - p$ is the pressure drop in the vortex which is proportional to $(\Gamma/r_c)^2$ and $\rho g \Delta H$ is a head drop representing viscous losses. Considering the increased Γ, associated with the controlled tip vortex, it is clear that from Eq. (3) that appropriate TEF control acts to decrease u_c. Furthermore, because the viscous losses in a promoted attached boundary layer (e.g., by a downward flap deflection) will be significantly less than those in a thicker separated boundary layer, the flap control therefore acts to further increase the centerline velocity by reducing the viscous head drop. It is therefore a combination of decreased pressure drop and increased head drop that seem to be jointly responsible for the lower axial velocities.

It is also worth to note that as the tip vortex of an oscillating wing is no longer circular in shape, a measure of the degree of distortion was defined so as to qualitatively quantify the degree of vortex distortion with TEF control. The determination of a shape distortion factor (SDF) was based on the isovorticity contour encompassing 90% of the vorticity. This level was chosen to avoid the arbitrary shape variations of the outermost contour levels due to low-level noise in the data. The SDF was determined by first discretizing the contour into numerous points, the radial distances r of which were defined relative to the vortex center (based on the location of peak vorticity), and then calculating the rms value of these radial locations using

$$\text{SDF} = \sqrt{\frac{\sum_{i=1}^{n}(r_i - \bar{r})^2}{n}}$$

The increased distortion of the vortex shape, compared to a baseline wing, with earlier flap actuation is evident (Fig. 5d). The negative TEF motion actuated at $t_s = 0\pi$ provided the most pronounced vortex distortion and displacement (Figs. 7a and 7b) as well. In general, the later the flap actuation the smaller the SDF. Also, note that due to the high distortion of the vortex shape, the critical values of the vortex core radius and the peak tangential velocity cannot be identified reliably. Nevertheless, typical distributions of the tangential velocity v_θ, mean axial velocity, and ζ across the vortex center (taken as the location of local maximum vorticity) along the y axis at $\alpha_u = 18^\circ$ and $\alpha_d = 11^\circ$ with and without TEF control are presented in Fig. 6 for reference only.

The influence of TEF motion on the tip vortex structure, in addition to the variation in ζ, ζ_{peak}, Γ_o, and u_c, can also be reinforced from the displacement of the vortex position, compared to a baseline wing (Figs. 7a and 7b). As discussed in Eq. (1), past investigations have shown that the change in the miss-distance d_{miss} of the BVI seems to be the major factor in reducing the blade-vortex interactions and BVI noise generation, and that it is less detrimental if the tip vortex can be somehow altered so that its strength is reduced or its core size substantially increased. The present results show that the positive TEF motion generally shifted the vortex further vertically upward (Fig. 7a), compared to a baseline wing, whereas a negative TEF motion gave rise to a substantial vertical downward shifting (well below that of a baseline wing) of the vortex center. The

additional vertical displacement, or equivalently increased d_{miss}, also implies a reduced blade-vortex interaction with lessened unsteady blade pressure fluctuations and, subsequently, a lowered BVI noise generation [as indicated by Eq. (1)]. The earlier the negative (positive) flap actuation, the larger the downward (upward) vertical shifting of the vortex. The $t_s = 0\pi$ and $\delta_{\max} = -7.5^\circ$ control case provided the most significant vertical displacement of the tip vortex of an oscillating wing; that is, the negative deflection was more effective in displacing the vortex vertically. Figure 7b further reveals that upward flap motion always shifted the vortex more inboard, especially during pitch-down, compared to a baseline wing, and that the later the flap actuation the more inboard the displacement of the vortex. For negative deflections, the z_c position was, however, observed to be shifted further outboard, compared to a baseline wing, especially during the pitch-up motion of the wing. The earlier the negative deflection the more significant the outboard shifting of the vortex center was.

Finally, the effect of TEF motion on the lift-induced drag coefficient C_{Di} was also examined. The C_{Di} was computed, based on the vorticity inferred from the measured velocity field, by using the Maskell method [24]. The vw-crossflow velocity vectors within the measurement plane were decomposed into a stream function $\psi(y, z)$ and a velocity potential $\phi(y, z)$ with the imposed boundary conditions requiring both ψ and ϕ to be zero on the edges of the measurement plane. The lift-induced drag D_i was then obtained by

$$D_i = \frac{1}{2}\rho_\infty \iint_{S\zeta} \psi\zeta \,\mathrm{d}y\,\mathrm{d}z - \frac{1}{2}\rho_\infty \iint_{S1} \phi\sigma \,\mathrm{d}y\,\mathrm{d}z \tag{4}$$

where ζ is the vorticity, the surface S_ζ is the region within $S1$ where the vorticity is nonzero, $\sigma(=\partial v/\partial y + \partial w/\partial z)$ is a source term, and the flow is incompressible. Figure 7c shows that similar to the observed variation in the Γ_o-α loop, the lift-induced drag coefficient was higher during pitch-up than during pitch-down. The upward, or positively, deflected TEF provided a further reduction in C_{Di} compared to a downward TEF motion, which increased C_{Di}. In other words, the downward, or negative, trailing-edge flap deflection delayed the trailing-edge flow separation and the dynamic lift stalling and rendered an increase in the lift force and Γ_o, compared to a baseline wing, but at the price of an increased C_{Di}.

Conclusions

The scheduled full-span trailing-edge flap controls, superimposed on a sinusoidally oscillating NACA 0015 wing, on the near-field tip vortex flow structure were investigated at $Re = 1.65 \times 10^5$. The larger the positive flap deflection the more efficient the C_l and $|-C_{m,\text{peak}}|$ reduction mechanism was, as a result of the suction pressure introduced on the lower surface of the control flap. The LEV formation and detachment were not significantly affected by the TEF motion, although the low pressure signature or footprint of the LEV was, however, reduced by the upward flap deflection. The TEF control was found to have a marked effect on location, strength, shape, axial velocity, and vorticity distribution of the tip vortex. The negative flap motion was found to be most effective in displacing the vortex position. In general, the earlier the actuation the larger the vortex displacement. Negative flap deflections strengthened the vortex, moved the centroid further outboard, decreased the peak vorticity ζ_{peak}, and increased the vortex size. The positive flap motions, however, resulted in a more concentrated tip vortex of reduced vortex strength Γ_o and moved the centroid further inboard, compared to an uncontrolled baseline wing. The positive flap deflection, however, produced less induced drag compared to a negative flap deflection. Both off- and on-surface flow measurements and visualizations are needed to better understand the phenomena reported here.

Acknowledgement

This work was supported by the Natural Science and Engineering Research Council (NSERC) of Canada.

References

[1] Hardin, J. C., and Lamkin, S. L., "Concepts for Reduction of Blade/Vortex Interaction Noise," *Journal of Aircraft*, Vol. 24, No. 2, 1987, pp. 120–125.

[2] Booth, E. R., "Experimental Observations of Two-Dimensional Blade-Vortex Interaction," *AIAA Journal*, Vol. 28, No. 8, 1990, pp. 1353–1359.

[3] Straus, J., Renzoni, P., and Mayle, R. E., "Airfoil Pressure Measurements During a Blade Vortex Interaction and a Comparison With Theory," *AIAA Journal*, Vol. 28, No. 2, 1990, pp. 222–228.

[4] Tung, C., Kube, R., Brooks, T. F., and Rahier, G., "Prediction and Measurement of Blade-Vortex Interaction," *Journal of Aircraft*, Vol. 35, No. 2, 1998, pp. 260–266.

[5] Wilder, M. C., and Telionis, D. P., "Parallel Blade-Vortex Interaction," *Journal of Fluids and Structures*, Vol. 12, No. 7, 1998, pp. 801–838.

[6] Tangler, J. L., "Experimental Investigation of the Subwing Tip and its Vortex Structure," NASA CR-3058, Nov. 1978.

[7] Liu, Z., Russell, J. W., Sankar, L. N., and Hassan, A. A., "A Study of Rotor Tip Vortex Structure Alteration Techniques," *Journal of Aircraft*, Vol. 38, No. 3, 2001, pp. 473–477.

[8] Muller, R. H. G., "Winglets on Rotor Blades in Forward Flight: A Theoretical and Experimental Investigation," *Vertica*, Vol. 14, No. 1, 1990, pp. 31–46.

[9] Gerontakos, P., and Lee, T., "Effect of Winglet Dihedral on a Tip Vortex," *Journal of Aircraft*, Vol. 43, No. 1, 2006, pp. 117–124.

[10] Brooks, T. F., Booth, E. R., Boyd, D. D., Splettstoesser, W. R., Schultz, K.-J., Kube, R., Niesl, G. H., and Streby, O., "Analysis of a Higher Harmonic Control Test to Reduce Blade Vortex Interaction Noise," *Journal of Aircraft*, Vol. 31, No. 6, 1994, pp. 1341–1349.

[11] Nguyen, K., "Active Control of Helicopter Blade Stall," *Journal of Aircraft*, Vol. 35, No. 1, 1998, pp. 91–98.

[12] Shen, J., and Chopra, I., "Swashplateless Helicopter Rotor with Trailing-Edge Flaps," *Journal of Aircraft*, Vol. 41, No. 2, 2004, pp. 208–214.

[13] Enenkl, B., Kloppel, V., Preibler, D., and Janker, P., "Full Scale Rotor with Piezoelectric Actuated Blade Flaps," *28th Europe Rotorcraft Forum*, Royal Aeronautical Society, London, U.K., 2002.

[14] Feszty, D., Gillies, E. A., and Vezza, M., "Alleviation of Airfoil Dynamic Stall Moments via Trailing-Edge-Flap Flow Control," *AIAA Journal*, Vol. 42, No. 1, 2004, pp. 17–25.

[15] Gerontakos, P., and Lee, T., "Active Dynamic-Stall Flow Control via a Trailing-Edge Flap," *AIAA Journal*, Vol. 44, No. 3, 2006, pp. 469–480.

[16] Rennie, R. M., and Jumper, E. J., "Experimental Measurements of Dynamic Control Surface Effectiveness," *Journal of Aircraft*, Vol. 33, No. 5, 1996, pp. 880–887.

[17] McCroskey, W. J., "Unsteady Airfoils," *Annual Review of Fluid Mechanics*, Vol. 14, Jan. 1982, pp. 285–311.

[18] Ramaprian, B. R., and Zheng, Y., "Near Field of the Tip Vortex Behind an Oscillating Rectangular Wing," *AIAA Journal*, Vol. 36, No. 7, 1998, pp. 1263–1269.

[19] Chang, J. W., and Park, S. O., "Measurement in the Tip Vortex Roll-Up Region of an Oscillating Wing," *AIAA Journal*, Vol. 38, No. 6, 2000, pp. 1092–1095.

[20] Lee, T., and Gerontakos, P., "Investigation of Flow Over an Oscillating Airfoil," *Journal of Fluid Mechanics*, Vol. 512, Aug. 2004, pp. 313–341.

[21] Chow, J. S., Zilliac, G. G., and Bradshaw, P., "Mean and Turbulence Measurements in the Near Field of a Wingtip Vortex," *AIAA Journal*, Vol. 35, No. 10, 1997, pp. 1561–1567.

[22] Leishman, J. G., *Principles of Helicopter Aerodynamics*, Cambridge Univ. Press, Cambridge, U.K., 2002, pp. 379–389.

[23] Batchelor, G. K., "Axial Flow in Trailing Line Vortices," *Journal of Fluid Mechanics*, Vol. 20, Dec. 1964, pp. 645–658.

[24] Maskell, E., "Progress Towards a Method for the Measurement of the Components of the Drag of a Wing of a Finite Span," RAE Rept. 72232, 1973.

N. Chokani
Associate Editor